A New High Resolution Thermal Detector Array

P1.1

Dillner, Ulrich; Riesenberg, Rainer
Institute for Physical High Technology
P.O.Box 100239, D-07702 Jena, Germany
Phone/Fax: +49-3641-206-312/399
E-mail: dillner@ipht-jena.de

Abstract

A new high resolution thermal detector staggered array is proposed where the two subarrays are not staggered *side by side* within the same plane as known, but *one upon the other* in a 3-D staggered arrangement. Thus the slits in the membrane of the first subarray act as apertures through which the radiation falls onto the second subarray.
The performance of the new thermal detector array arrangement is calculated using thermal finite element analysis. The influence of the thermal intra- and inter-subarray cross-talk on the resolution in dependence on some geometrical dimensions of the array is presented.

Introduction

Linear thermal infrared detector arrays are known as linear arrangements of a number of pixels comprised by single element thermal sensors. They are useful for applications in spectrometers to simultaneously register a spectral distribution in dependence on wavelength or for applications in thermal imaging.

Generally, the resolution of these devices increases with the number of pixels. Hence, in the context of miniaturization, an increased pixel density will improve the resolution. On the other hand, the pixel density, i.e., number of pixels per unit length of the linear array which is equal to the inverse pixel pitch, can not be increased arbitrarily due to technologically determined minimal structural dimensions of the pixel and due to the thermal cross-talk. In order to double the resolution despite the limitation of the pixel density by minimal structural dimensions the usual simple in-line arrangement of all pixels of the linear array [1-7] has been replaced by a staggered arrangement, i.e., an arrangement of two subarrays within a *single plane* staggered by one half of the pitch of these subarrays [8-12], cf. Fig. 1. With p being the pitch of the subarray the effective pitch of the staggered array is p_{eff} = p/2. For reducing the thermal cross-talk between adjacent pixels situated on the same membrane this membrane can be slit between the pixels, e.g. by dry ion etching [7, 11]. However, this solution for improving the resolution of a thermal detector array has the disadvantage that a part of the radiation hitting the array is wasted reducing the efficiency of the array.

Therefore, a new high resolution thermal detector staggered array is proposed where the two (or more) subarrays are not staggered *side by side* within the same plane but *one upon the other* [13]. Thus the slits in the membrane of the first subarray act as apertures through which the (otherwise wasted) radiation falls onto the second subarray. In this work the performance of the new thermal detector array arrangement is

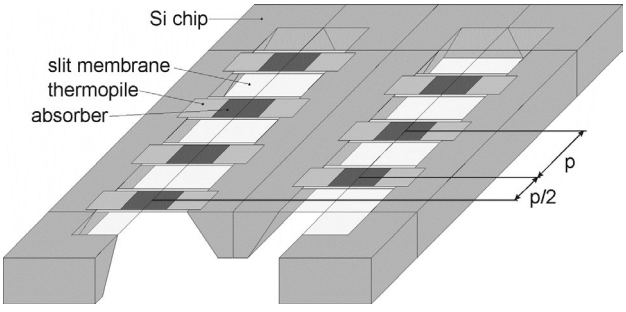

Figure 1. Schematic representation of a state-of-the-art 2D-staggered array arrangement.

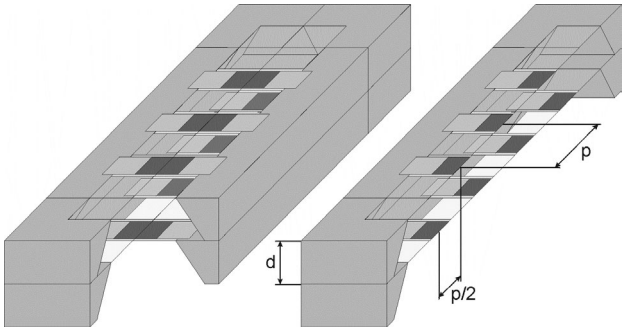

Figure 2. Schematic representation of the new 3D-staggered array arrangement with two subarrays, p: subarray pitch, d: vertical distance between the two membranes.

calculated using thermal finite element analysis (FEA). Performance and layout dimensions are discussed. The influence of the thermal intra- and inter-subarray cross-talk on the resolution in dependence on the pixel pitch and the subarray membrane spacing is presented.

Sensor Array Design

The design of the subarray is similar as published in [11]: A free-standing stress-compensated membrane made by anisotropic etching of a Si wafer covered with a 0.8 µm thick silicon oxinitride (SiON) layer serves as a substrate for the thermopiles patterned microlithographically by wet chemical etching. The thermopiles are formed by thin films of 0.4 µm thickness using n-type $Bi_{0.87}Sb_{0.13}$ against p-type Sb as thermocouple materials with a Seebeck coefficient *S*=135 µV/K per couple. Each thermopile is covered by an absorption layer. There is a pixel separating region between two pixels which is essentially formed by a slit in the membrane to reduce thermal cross-talk. The n-type and the p-type legs of the thermopiles are arranged one on the top of the other using a multi-layer technology including photoresist passivation layers [14]. This arrangement has the advantage of doubling the package density of the thermocouple legs. The approximate minimal structural dimensions of the thermocouples forming the thermopiles are a width of 8 µm and a spacing of 6 µm each. The complete array is composed of two equal-type subarrays staggered *one upon the other* in a 3-D staggered arrangement, cf. Fig. 2.

Thermal Analysis

A 3-D finite element analysis (FEA) was performed using the FEA code ANSYS® to simulate the stationary and transient temperature distribution. Two variants of the FEA modeling region are depicted schematically in Fig. 3. The modeling region comprises a quarter (due to symmetry) of three pixels of both subarrays as well as the gas-filled space above and below the selected pixels. The silicon rim, the header and the cap are not included in the FEA modeling region, since they are regarded as heat sinks at the temperature of the surroundings T_U. The central pixel denoted by "1" is loaded by a heat flux equivalent to the incident infrared radiation while the adjacent pixels are not loaded but receive the thermal cross-talk from the central pixel. The adjacent pixel on the same membrane as the central pixel is denoted by "2" the adjacent pixel on the other membrane is denoted by "3". The FEA modeling region is subdivided in regions of different material properties: absorber, thermopile, membrane and gas filling (N_2). The thin-film thermal conductivity and heat capacity data for the various layers including the self-supporting membrane, the thermopiles and photoresist insulation published in [15] were used in the calculations.

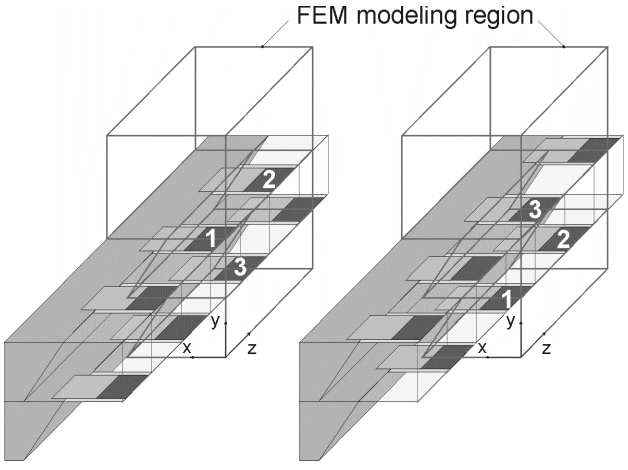

Figure 3. Schematic representation of the FEA modeling region of the 3D-staggered array arrangement. Left the central pixel (1) is located on the upper membrane, right on the lower membrane. The adjacent pixels (2) and (3) are on the same and the other membrane as (1), respectively.

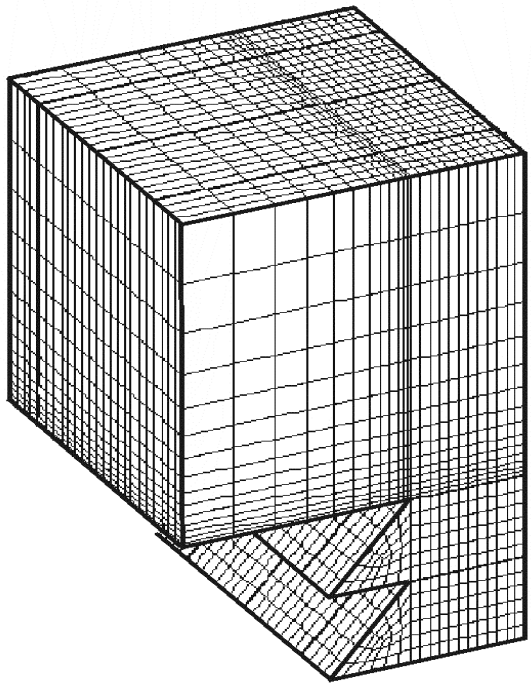

Figure 4. 3D FE model of the 3D-staggered array arrangement.

Note that the thermal conductivity as well as the heat capacity per unit volume of the multilayer stacks are calculated by a weighted addition of the individual data of each layer (lumped model) [15]. The FE model corresponding to the modeling region of Fig. 3 and showing the finite elements is represented in Fig. 4.

FEA Results

The stationary temperature distribution given in Fig. 5 may serve as an example result for the FEA calculations carried out. Here p = 0.4 mm and d = 0.2 mm. The membrane and absorber widths are 1 mm and 0.5 mm, respectively. The distance between the upper membrane and the sensor cap is 2 mm. The central pixel on the upper membrane receives a heat flux of 100 W/m².

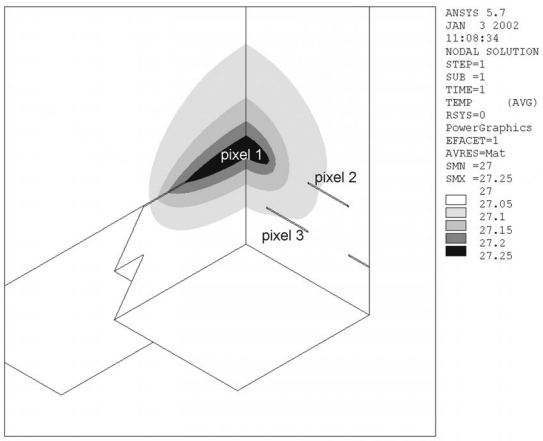

Figure 5. Stationary temperature distribution of a 3D-staggered array arrangement with the irradiated pixel (1) located on the upper membrane. The adjacent pixels (2) and (3) are influenced by the "thermal cloud" arising from the irradiated pixel (irradiance: 100 W/m²).

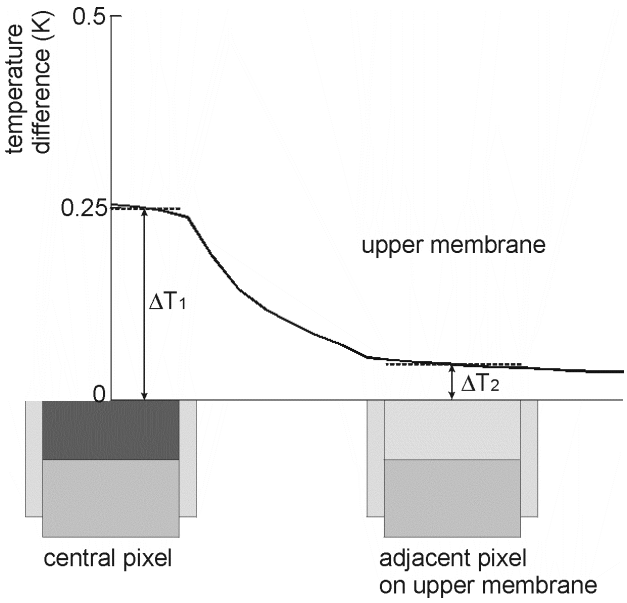

Figure 6. Stationary temperature distribution along the line in the middle of the upper membrane (central pixel irradiance: 100 W/m²).

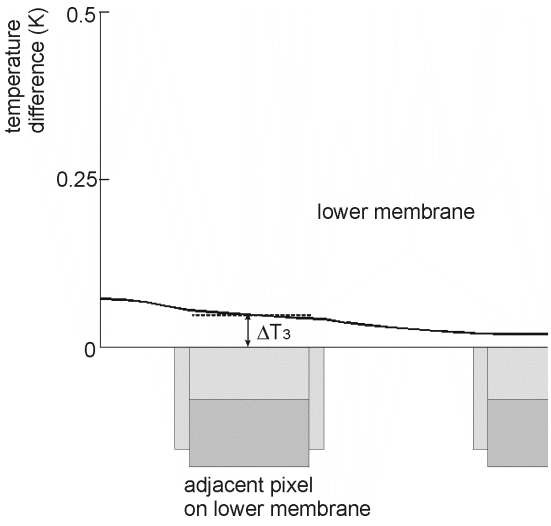

Figure 7. Stationary temperature distribution along the line in the middle of the lower membrane.

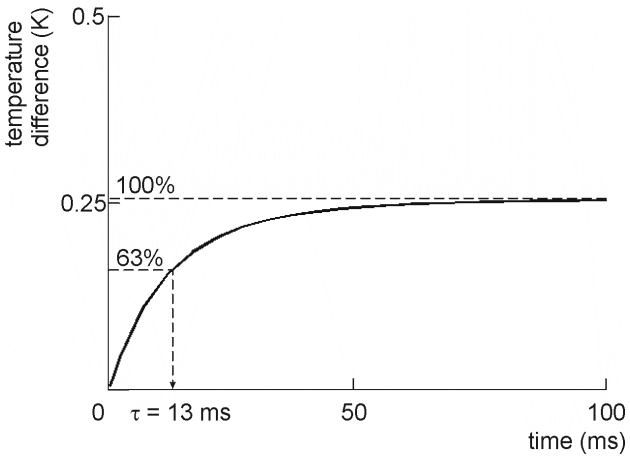

Figure 8. Transient temperature distribution at the midpoint of the irradiated pixel and determination of the time constant τ.

Figs. 6 and 7 represent the stationary temperature distributions along two characteristic lines of the 3D-staggered array. From these distributions the intra-subarray cross-talk C_2 and the inter-subarray cross-talk C_3 can be determined: $C_i = \Delta T_i / \Delta T_1$, i = 2, 3. Here ΔT_i is the mean temperature difference between the hot and cold thermocouple junctions of the i-th pixel thermopile. With ΔT_1 = 0.247 K, ΔT_2 = 0.047 K and ΔT_3 = 0.049 K the cross-talk is C_2 = 0.19 and C_3 = 0.20. From the value of ΔT_1 the signal voltage U_s can be calculated employing $U_s = nS\Delta T_1$, where n is the number of thermocouples of the thermopile. With n = 26 for the given p deduced from the minimal structural dimensions of the thermocouples we find U_s = 0.87 mV. The transient temperature distribution, cf. Fig. 8, can be used to determine the thermal time constant of the array.

The procedure described above was carried out while varying the subarray pitch p between 0.1 and 2 mm and the subarray membrane spacing d between 0.1 and 1 mm. The results are given in Figs. 9 - 13. These results are based on the FEA model with the irradiated pixel on the upper membrane (cf. left part of Fig. 3).

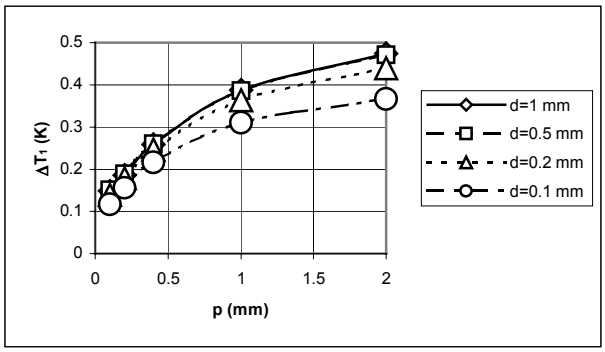

Figure 9. Mean temperature difference between the hot and cold junctions of the pixel irradiated at 100 W/m² in dependence on p and d.

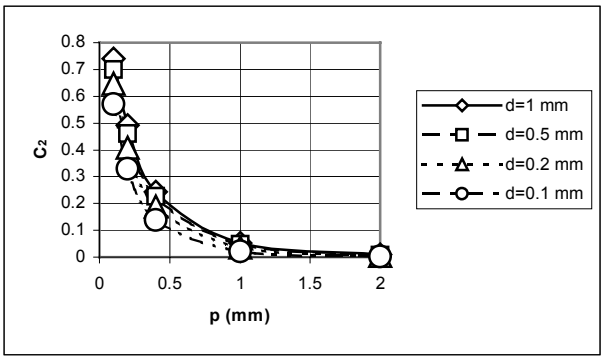

Figure 10. Intra-subarray cross-talk in dependence on p and d.

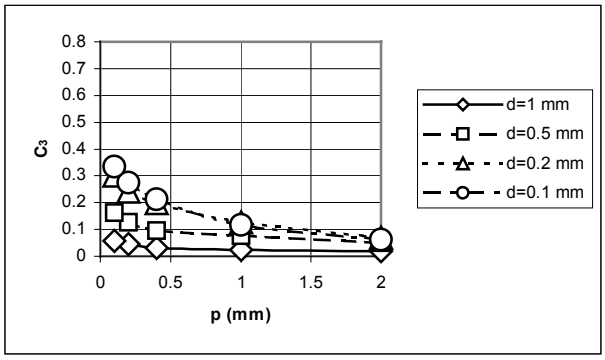

Figure 11. Inter-subarray cross-talk in dependence on p and d.

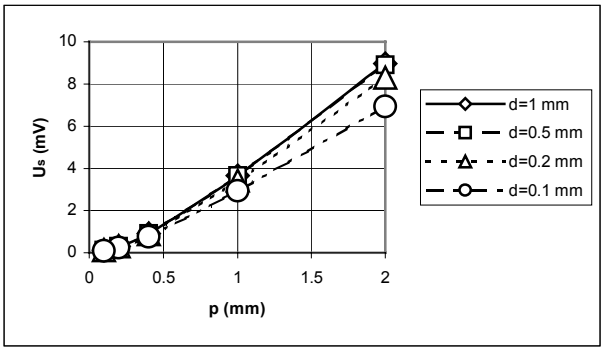

Figure 12. Signal voltage at an irradiance of 100 W/m² in dependence on p and d.

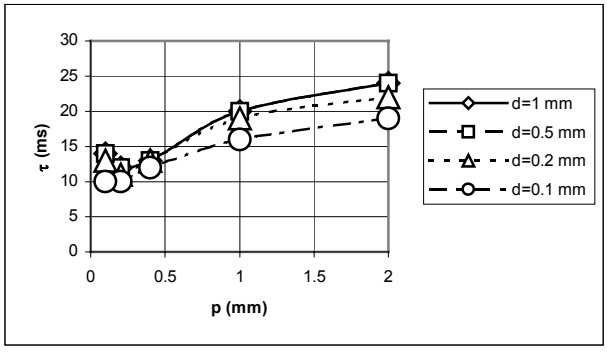

Figure 13. Time constant in dependence on p and d.

Similar results were obtained employing the model with the irradiated pixel on the lower membrane (cf. right part of Fig. 3). However, due to the better coupling between the lower membrane and the heat sink formed by the header, the mean temperature differences between the hot and cold junctions of the irradiated pixel, the signal voltages and time constants are lower in this case, especially for small values of d. Fig. 14 shows the explicit results for the signal voltage in comparison to Fig. 12. The corresponding graphs of the mean temperature difference between the hot and cold junctions of the irradiated pixel and of the time constant are not explicitly presented here for want of space. While the inter-subarray cross-talk is nearly the same as in the

case where the irradiated pixel is located on the upper membrane, the intra-subarray cross-talk differs more between the two cases, cf. Fig. 15 in comparison to Fig. 10.

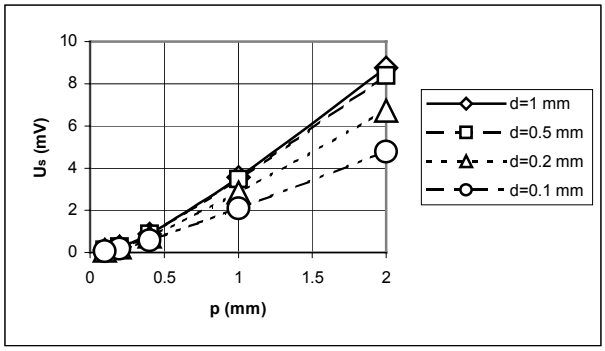

Figure 14. Signal voltage at an irradiance of 100 W/m² in dependence on p and d by using the model with the irradiated pixel on the lower membrane.

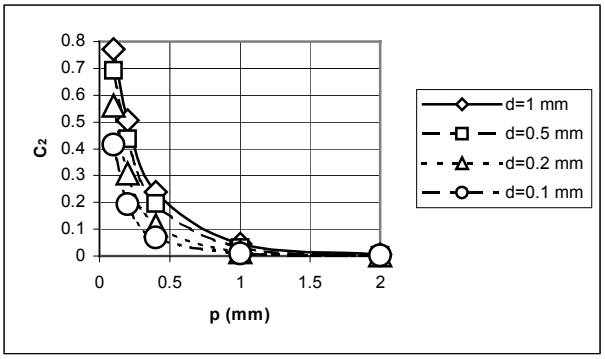

Figure 15. Intra-subarray cross-talk in dependence on p and d by using the model with the irradiated pixel on the lower membrane.

Discussion of Results

The signal voltage at 100 W/m² irradiance (cf. Figs. 12 and 14) may serve as a performance parameter of the array. It depends very strongly on the pitch $p = 2p_{eff}$ and falls down to values of about 0.1 mV at an effective pitch of the staggered array of 50 µm (p = 0.1 mm). Since, for applications of the array in spectrometers, a high spectral resolution is desirable and the spectral resolution is proportional to the effective pixel density, a low p_{eff} is needed to achieve this goal. Because a low pitch is at the expense of signal voltage a trade-off between spectral resolution and signal voltage has to be made.

Another problem related to a low pitch is the increase in cross-talk (cf. Figs. 10, 11 and 15). With the N_2 gas filling at normal pressure assumed in the calculations the cross-talk C_2 can reach very high values (up to 0.77) at p_{eff} = 50 µm. Off course, the cross-talk is at the expense of spectral resolution. Thus the envisioned goal of obtaining a high spectral resolution by lowering the effective pixel pitch of the array is obstructed by a high thermal cross-talk. If we set a limit of, say, $C_i = 0.25$ then it is found from Figs. 10, 11 and 15 that effective pitches down to 0.2 mm (p =0.4 mm) are within this limit. For smaller pitches a vacuum encapsulation of the array is favorable leading to a negligible thermal cross-talk in case of slit membranes. For comparison the example represented in Figs. 5 to 8 was recalculated assuming vacuum instead of N_2 gas filling. The results are ΔT_1 = 1.88 K, $C_2 = C_3 = 0$, τ = 85 ms and U_s = 6.5 mV. Hence, apart from preventing cross-talk, vacuum housing clearly improves the signal voltage at the expense of the response time. But vacuum encapsulation may lead to some technological problems. The behavior characteristic for thermal sensors that an increase in signal voltage results in a corresponding rise of the time constant is also found when comparing Fig. 12 and 13. A consequence of an increase of time constant is a rise of measurement time and a reduced throughput.

Interestingly, while the behavior of the intra- and inter-subarray cross-talk with respect to the variation of p is the same (falling with rising p), the behavior is diametrical with respect to the variation of d (rising with rising d concerning the intra-subarray cross-talk and falling with rising d concerning the inter-subarray cross-talk). This can be exploited to design an 3D-staggered array with a balanced cross-talk characteristics, i.e. $C_2 \sim C_3$. However, the vertical distance between the two membranes d is limited by the depth of focus of the optics illuminating the array. If d is too large the resulting blur will degrade the resolution.

Conclusion

A new high resolution thermal detector staggered array was proposed. Two or more subarrays are stacked one upon the other in a 3-D staggered arrangement. In the case of two stacked subarrays, the resulting effective pitch equals to half the pitch of the subarrays which potentially yields a doubling of the resolution.
However, the thermal cross-talk between adjacent pixels can reduce this potential. Therefore, in case that a vacuum housing of the array is not realized due to the needs of a fast response time or for technical reasons, the geometry of the arrangement, especially the subarray pitch and the subarray membrane spacing, can be optimized with respect to cross-talk in order to obtain a reasonable trade-off between spatial resolution and signal voltage.

References

[1] P.M. Sarro, H. Yashiro, A.W. v. Herwaarden, S. Middelhoek, An integrated thermal infrared sensing array, *Sensors and Actuators, 14* (1988) 191-201

[2] R. Lenggenhager, H. Baltes, T. Elbel, Thermoelectric infrared sensors in CMOS technology, *Sensors and Actuators, A37-38* (1993) 216-220

[3] R. Köhler, N. Neumann, G. Hofmann, Pyroelectric single-element and linear-array sensors based on P(VDF/TrFE) thin films, *Sensors and Actuators, A45* (1994) 209-218

[4] H. Jerominek, F. Picard, N.R. Swart, M. Renaud, M. Levesque, M. Lehoux, J.S. Castonguay, M. Pelletier, G. Bilodeau, D. Audet, T.D. Pope, P. Lambert, Micromachined uncooled VO_2-based IR bolometer arrays, *Proc. SPIE, 2746* (1996) 60-71

[5] C.M. Travers, A. Jahanzeb, D.P. Butler, Z. Celik-Butler, Fabrication of semiconducting YBaCuO surface-micromachined bolometer arrays, *J. Microelectromech. Systems, 6* (1997) 271-276

[6] M. Simon, J. Schieferdecker, M. Schulze, R. Gottfried-Gottfried, M. Müller, R. Jähne, Linear thermopile sensor array for contactless temperature measurement, *Proceedings of Sensor '97, 8th International Trade Fair and Conference for Sensors, Transducers & Systems, Vol. II*, Nürnberg, 1997, 83-88

[7] M.C. Foote, E.W. Jones, T. Caillat, Uncooled thermopile infrared detector linear arrays with detectivity greater than 10^9 $cmHz^{1/2}/W$, *IEEE Trans. on Electron Dev., 45* (1998) 1896-1902,

[8] I.H. Choi, K.D. Wise, A silicon-thermopile-based infrared sensing array for use in automated manufacturing, *IEEE Trans. on Electron Devices, ED-33* (1986) 72-79

[9] W. Schnelle, U. Dillner, S. Poser, A linear thermopile infrared sensing array, *VDI-Berichte, 982,* (1992) 261-264

[10] W.G. Baer, K. Najafi, K.D. Wise, R.S. Toth, A 32-element micromachined thermal imager with on-chip multiplexing, *Sensors and Actuators, A48* (1995) 47-54

[11] E. Kessler, U. Dillner, V. Baier, J. Müller, A 256 pixel linear thermopile array using materials with high thermoelectric efficiency, *Proceedings of the XVI International Conference on Thermoelectrics*, Dresden, 1997, 734-737

[12] J.-P. Krebs, O. Brunel, C. Guerin, D. Guillon, J.M. Niot, A new infrared static earth sensor for micro and nano-satellites, *2nd Round Table on Micro/Nano Technologies for Space*, ESTEC (Noordwijk), 15-17 October 1997, 187-197.

[13] Patent pending.

[14] F. Völklein, A. Wiegand, High sensitivity and detectivity radiation thermopiles made by multi-layer technology, *Sensors and Actuators, A24* (1990) 1-4.

[15] U. Dillner, Thermal modeling of multilayer membranes for sensor applications, *Sensors and Actuators, A41-A42* (1994) 260-267.